ChemPubSoc Europe

DOI: 10.1002/batt.201800119

BATTERIES & SUPERCAPS
Articles

Special Issue

Peroxide Yield of the (001) $La_{0.6}Sr_{0.4}MnO_3$ Surface as a Bifunctional Electrocatalyst for the Oxygen Reduction Reaction and Oxygen Evolution Reaction in Alkaline Media

Lennart Köhler,[a] Lukas Szabadics,[a] Christian Jooss,[a] and Marcel Risch*[a]

Active and stable bifunctional electrocatalysts are required for large-scale deployment of rechargeable metal-air and metal-O_2 batteries. This is hindered by the large overpotentials of the oxygen evolution reaction (OER) and oxygen reduction reaction (ORR) in alkaline media, where peroxide is an undesired side product. We study the suitability of epitaxial (001)-oriented $La_{0.6}Sr_{0.4}MnO_3$ perovskite surfaces as a bifunctional catalyst using a rotating-ring disk electrode (RRDE) assembly and focus particularly on the selectivity of the ORR. The peroxide yield is above 50% during ORR-only investigations in the scan range of 0.69 to 0.99 V vs. RHE where the CV traces are reproducible. In contrast, the peroxide yield is drastically reduced during OER-ORR cycling where a peroxide yield below 10% is reached during the ORR in the scan range of 0.74 V to 1.74 V vs. RHE. Our study highlights the importance of the electrode history and thus clearly demonstrates that separate studies of the OER and ORR are insufficient to optimize bifunctional electrocatalysts.

1. Introduction

All rechargeable metal-O_2 and metal-air batteries rely on high performance of their oxygen electrode (i.e. the positive electrode). Thus, the high overpotential of the two reactions of oxygen electrocatalysis, namely the oxygen reduction reaction (ORR) and oxygen evolution reaction (OER) is a key challenge in the development of practical reachable metal-O_2 and metal-air batteries.[1–12] Oxygen electrocatalysis has attracted considerable scientific interest in the last decades, which led to high performance in prototype devices[13–15] and fundamental insight from materials testing in half cells such as the descriptor approach.[1,16–18] Single crystalline thin films are ideally suited to develop guidelines for practical catalyst materials with high surface area because these thin films have smooth and flat surfaces of a controlled orientation and do not need additives such as carbon or binders that are used in composite electrodes.[3,9,18] Thin film metal oxides with the perovskite structure have been most extensively studied in this context as they allow variation of the chemical composition without significant impact on the structural framework.[19]

The $La_{1-x}Sr_xMnO_{3\pm\delta}$ perovskite system includes some of the most intrinsically active oxides for the ORR,[18,20] e.g., $LaMnO_{3+\delta}$ powder[17] and (001)-oriented $La_{0.67}Sr_{0.33}MnO_3$ thin films.[21] The ORR has not previously been studied on $La_{0.6}Sr_{0.4}MnO_3$ thin films of any orientation but the composition is close to the maximum identified by Stoerzinger et al.[21] for the $La_{1-x}Sr_xMnO_3$ system. Furthermore, the OER activity of (001)-oriented $La_{0.6}Sr_{0.4}MnO_3$ is comparable to that of (110)-oriented IrO_2.[22] In addition, manganese is very abundant in the earth's crust and the cost of its oxides is low. The combination of these properties makes the $La_{1-x}Sr_xMnO_{3\pm\delta}$ perovskite system an excellent candidate material for the oxygen electrode of a metal-air or metal-O_2 cell. Single crystalline and polycrystalline $La_{1-x}Sr_xMnO_3$ films with x between 0.0 and 0.7 have been previously studied for the oxygen reduction[21,23–26] and oxygen evolution[22,25,27] reactions or both.[25] However, the reproducibility of the CV traces and the stability of the material during the harsh conditions of both reactions must also be considered to realize practical devices.

The aspects of reproducibility and stability have received significantly less attention as compared to catalytic studies, particularly for thin films. One of us has previously studied the changes of (001)-oriented $La_{0.8}Sr_{0.2}MnO_3$ thin films during 100 cycles between 1.15 and 1.70 vs. RHE (OER range) and then 100 cycles between 1.00 and 0.65 V vs. RHE (ORR range).[25] Using this protocol, the activity of the OER increased with cycling, while the activity of the ORR decreased. However, the decrease during the ORR could be alleviated by depositing $Ba_{0.5}Sr_{0.5}Co_{0.8}Fe_{0.2}O_{3-\delta}$ on $La_{0.8}Sr_{0.2}MnO_3$. It was hypothesized that the manganese valence may change during the experiments but the influence of the scan range, which enables or disables manganese redox, was not investigated.

Selectivity is another related aspect that is understudied as compared to activity studies. Both the OER[28] and ORR[29] can yield peroxide in addition to the desired products of oxygen and hydroxide/water. The electrochemical methods for determination of the peroxide yield are well-established but were not adapted for the study of $La_{1-x}Sr_xMnO_3$ films until very recently.

[a] L. Köhler, L. Szabadics, Prof. C. Jooss, Dr. M. Risch
Georg-August Universität Göttingen
Institut für Materialphysik
Friedrich-Hund-Platz 1, 37077 Göttingen
E-mail: mrisch@material.physik.uni-goettingen.de

Supporting information for this article is available on the WWW under https://doi.org/10.1002/batt.201800119

An invited contribution to a Special Issue on Bifunctional Catalysts for Metal-Air Batteries

Miyahara et al.[24] studied polycrystalline $La_{0.8}Sr_{0.2}MnO_3$ on Pt disks. In contrast to powders, the limiting current was not reached, and the rotation rate had little influence on the measured currents. Kan et al.[23] designed a holder to rotate epitaxial (001)-oriented $La_{0.67}Sr_{0.33}MnO_3$ thin films on conventional square substrates, yet their film behaved similar to that of Miyahara et al.[24] Thus, it was not possible to determine the peroxide yield or number of transferred electrons in either study using the established Levich or Koutecký-Levich analyses. Consequently, the peroxide yield of the $La_{1-x}Sr_xMnO_3$ perovskites was only determined on composite electrodes of $La_{1-x}Sr_xMnO_3$ powders,[30] where carbon may act as an additional catalyst or co-catalyst.[3,9,31–33]

In this study, we used our recently developed thin film rotating-ring disk electrode setup[22] to study the ORR on (001)-oriented $La_{0.6}Sr_{0.4}MnO_3$. In contrast to previous studies,[23,24] the Pt ring electrode enabled us to directly quantify the peroxide yield of the $La_{0.6}Sr_{0.4}MnO_3$ surface in the absence of any additives. We further investigated the influence of the scan range on the peroxide yield as well as on the reproducibility of ORR measurements. Dwindling ORR currents were found at voltages lower than 0.69 V vs. RHE during investigations of the ORR and for any voltage boundary during bifunctional cycling between OER and ORR. Thus, our study demonstrated the importance of the electrode history of the scan range for bifunctional investigations.

2. Results and Discussion

$La_{0.6}Sr_{0.4}MnO_3$ films grew epitaxially on a (001)-oriented Nb-doped $SrTiO_3$ substrates because only the reflections of the {001} family were detected in off-axis XRD (Figure 1a). The $La_{0.6}Sr_{0.4}MnO_3$ films have the expected double peaks where one matches that of the substrate and the other peak at higher angle was due to the slightly shorter pseudo-cubic lattice parameter of $La_{0.6}Sr_{0.4}MnO_3$ (inset of Figure 1a). The experimental lattice parameter a of cubic crystal systems can be determined by the average ratio of the interplanar distance d (from Bragg's law) to $(h^2+k^2+l^2)^{1/2}$ where hkl are the Miller indices. Using this approach and the reflections in Figure 1a, we obtained a lattice parameter of $a_{STNO}=3.906(1)$ Å, which was identical to undoped $SrTiO_3$ ($a_{STO}=3.905$ Å[34]). The pseudo-cubic lattice parameter of the LSMO film was approximated as $a_{LSMO,pc}=3.828(1)$ Å, which agrees well with the out-of-plane lattice parameter of previously prepared films of around 3.83 Å and might indicate a slight manganese excess.[27]

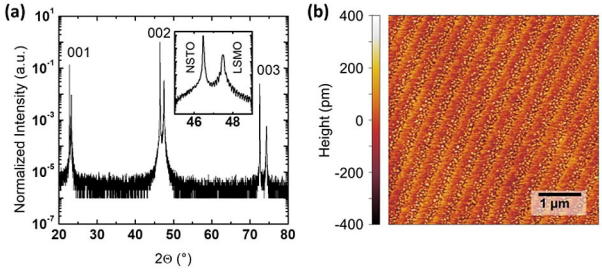

Figure 1. Pre-characterization of the $La_{0.6}Sr_{0.4}MnO_3$ (LSMO) thin film. a) Out-of-plane XRD of LSMO on Nb-doped $SrTiO_3$ (STNO). (b) AFM image of the film demonstrating a very low roughness of the order of a unit cell step.

Atomic force microscopy (AFM) showed that the produced films were very flat (Figure 1b and Figure S1), yielding an average root-mean square (RMS) of 0.1 nm and roughness factors better than 1.00009 (Figure S1; definition in Experimental Section). Both values agree with the averages 0.116(25) nm and 1.00009(10) of previously prepared films.[22] The film had a terraced surface that reflects the terrace structure of the substrate. The AFM images supported step flow growth where new layers nucleate at both on the terrace and the terrace steps, which explains the observed islands (Figure 1b). We note that the films studied here have a higher density of islands at the terrace edge as compared to typical film prepared previously,[22] which however did not affect the parameters of the surface morphology.

The physical properties of the produced films are summarized in Table S1 and equal those in our previous studies where additional characterization and discussion may be found.[22,27,35] In particular, Scholz et al.[22,27] previously studied (001)-oriented $La_{0.6}Sr_{0.4}MnO_3$ in scan ranges including the OER (i.e., 1.10 V to 1.75 V vs. RHE) where aspects of stability were also extensively covered. For this reason, we will refer the reader to these previous studies and focus on the ORR in a typical scan range and ORR during bifunctional cycling between the OER and ORR.

The shape of the CV on $La_{0.6}Sr_{0.4}MnO_3$ disks depended on the used scan range for bifunctional cycling between the OER and ORR. We recorded CVs in selected ranges between 0.59 and 1.74 V vs. RHE in Ar-saturated 0.1 M NaOH (Figure 2) on a $La_{0.6}Sr_{0.4}MnO_3$ electrode that was previously cycled 100 times between the OER and ORR (Figure S2a). No redox peaks or catalytic waves were found in the range between 0.59 and 1.14 V vs. RHE (denoted **1** in Figure 2). In the range between 1.14 and 1.49 V vs. RHE (denoted **2** in Figure 2), there was a broad double peak in anodic direction with charge of 40 µC

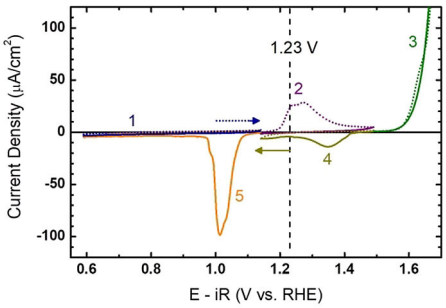

Figure 2. Cyclic voltammetry of a $La_{0.6}Sr_{0.4}MnO_3$ thin film in various scan ranges showing that the observed manganese redox depends on the history of the electrode. Numbers indicate the sequence of the measurements, which were performed in Ar-saturated 0.1 M NaOH at 10 mV/s and 1600 rpm. Arrows indicate the scan direction and the dashed line indicates the equilibrium potential of oxygen electrocatalysis.

(dotted line), but no corresponding reduction in the cathodic scan (solid line). The voltage of the peak at lower voltage equals the overpotential of oxygen electrocatalysis, namely 1.23 V vs. RHE. The range between 1.49 and 1.74 V vs. RHE (denoted **3** in Figure 2) also showed a shoulder with charge 15 μC in anodic direction and no corresponding feature in cathodic direction. In addition, the catalytic wave due to the OER was found in this range. When the range between 1.14 and 1.49 V vs. RHE (denoted **4** in Figure 2) was reinvestigated after oxygen evolution, we found a redox peak of charge −12 μC in cathodic direction but not in anodic direction. When the initial range of 0.59 and 1.14 V vs. RHE (denoted **5** in Figure 2) was revisited, a pronounced redox peak of charge −63 μC was identified in cathodic direction, again with no counterpart in the anodic scan. No redox peaks except the catalytic wave were observed during a 2nd cycle in the ranges discussed above (Figure S2b). The observed redox peaks thus depend strongly on the history of the electrode and the used scan range. Moreover, the sum of the anodic charges was 55 μC while that of the cathodic charges was −75 μC, which indicates that our film was likely reduced after the experiment, i.e., irreversibly modified.

We assigned the observed peaks to manganese redox reactions, which are well studied in literature,[36] albeit not for perovskite oxides. The expected nominal valence of manganese in $La_{0.6}Sr_{0.4}MnO_3$ is $Mn^{3.4+}$. Yet, since the electrode was previously cycled and we found a higher excess reductive charge in the investigated range, our sample was likely reduced below the nominal valence. The double peak in range **2** could be caused by different redox potentials of manganese on the terraces and at the edge of the terraces as often found for the better studied single crystals of metals, e.g. Pt.[37–39] The sequence and charges of the observed peaks suggested coupling of the peaks in ranges **2** and **5** as well as those in **3** and **4**. We assigned the peak in range **2** to Mn^{2+} to Mn^{3+} oxidation, the shoulder in range **3** to Mn^{3+} to Mn^{4+} oxidation, the peak in range **4** to reduction of Mn^{4+} to Mn^{3+}, and finally the peak in range **5** to Mn^{3+} to Mn^{2+} reduction. These assignments are supported by *in situ* X-ray absorption spectroscopy (XAS), where these redox reactions were observed on electrodeposited[29,40] and powdered[41] simple manganese oxides in similar ranges. We note that the exact value of the redox potential depends on the crystal structure and surface site, which is yet unknown for our (001)-$La_{0.6}Sr_{0.4}MnO_3$ surfaces. Mn^{2+} is not found in proper perovskite structures ($ABO_{3-\delta}$) with average A valence $\geq 2+$, yet it relates to oxygen vacancies ($\delta > 0$) or other point defects at the surface.[23,42–45] The electrochemical formation of these oxygen vacancies was directly observed on a related manganese oxide thin film by TEM[46] and *in situ* TEM during oxygen evolution.[47] Moreover, this valence is also found in the bulk of oxides with ordered oxygen vacancies related to perovskites such as Brownmillerite and double perovskites. Kan et al.[23] proposed that oxygen vacancies are formed on epitaxial films with comparable composition of $La_{0.67}Sr_{0.33}MnO_3$ during the ORR, which they support by *ex situ* XAS. Moreover, our assignment of (local) reduction below Mn^{3+} agrees with the assignment of Celorrio et al.[48–50] for perovskite powders also based on *ex situ* XAS. In summary, our analysis and comparison to literature supports that the (001)-$La_{0.6}Sr_{0.4}MnO_3$ surface undergoes redox reactions in the voltage range that covers bifunctional cycling between the OER and ORR.

The product yield was probed electrochemically using the ring of an RRDE set to 1.2 V vs. RHE. At this potential, positive current indicated peroxide production, while negative current indicated manganese dissolution as permanganate (Figure S3). At fixed ring voltage, the scan range of the disk was systematically changed by reducing the lower scan boundary. Selected disk current densities in cathodic direction and the corresponding ring currents for the lower boundaries of 0.74, 0.59 and 0.39 V vs. RHE are shown in Figure 3. Ring and disk currents are

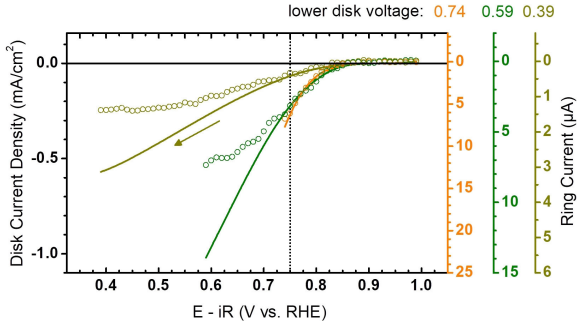

Figure 3. Voltage sweep of a $La_{0.6}Sr_{0.4}MnO_3$ disk (lines) in selected scan ranges during the 2nd cycle and the corresponding ring currents (circles) at 1.20 V vs. RHE smoothed by a 10 pt moving box average. The measurements were performed in O_2-saturated 0.1 M NaOH at 10 mV/s and 1600 rpm. The arrow indicates the cathodic scan direction. The vertical dotted line indicates the threshold voltage where the disk and ring currents deviate.

proportional during the entire range only for the lower boundary of 0.74 V. For the other shown scan ranges, the ring current deviates from the disk current at disk voltages lower than about 0.75 V vs. RHE. In addition, the scaling constant between ring and disk currents decreased even for voltages above 0.75 V (which can be seen best at decreasing maximum value on the right y-axes in Figure 3). Therefore, the irreversible changes of the product yield during previous cycles, i.e., the history of the electrode, was probed at any voltage above 0.75 V, while each voltage below 0.75 V vs. RHE probes the combined changes of the electrode history and additional voltage-dependent modifications.

We systematically studied the changes in the CV traces upon reducing the lower scan boundary in the ORR region, where the upper scan boundary was fixed at 0.99 V vs. RHE and the lower scan boundary was reduced from 0.79 to 0.39 V vs. RHE in 50 mV steps (Figure 4a) The traces during the 2nd cycle were similar up to and including a lower disk voltage boundary of 0.69 V vs. RHE. In this range, the voltages of the $La_{0.6}Sr_{0.4}MnO_3$ disk were between 0.81 and 0.82 V vs. RHE at −40 μA/cm², which fell within the expected range of 0.81 ($La_{0.5}Sr_{0.5}MnO_3$) to 0.85 V vs. RHE ($La_{0.67}Sr_{0.33}MnO_3$) reported by Stoerzinger et al.[21] When the lower boundary was reduced below 0.69 V, the magnitude of the current densities was lowered and the cathodic and anodic scans showed hysteresis for voltages

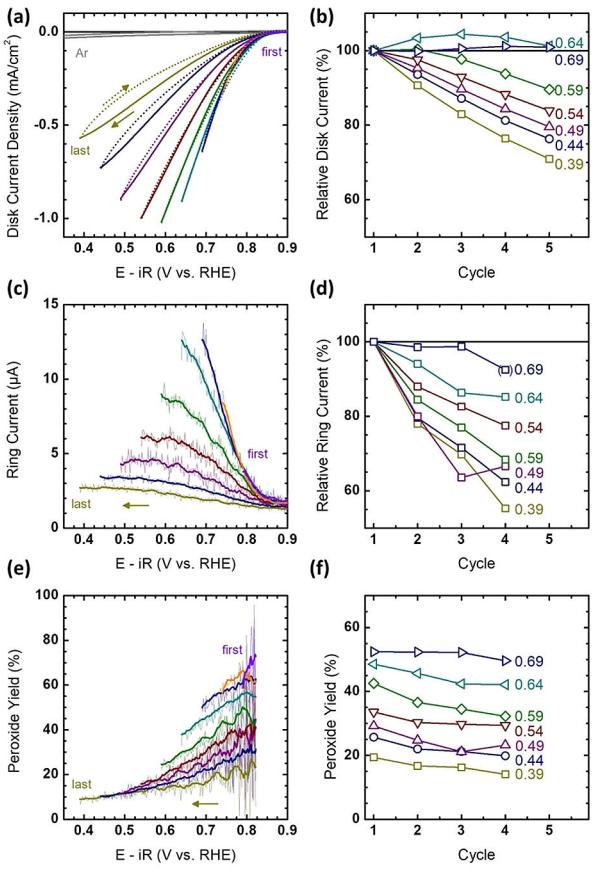

Figure 4. Identification of a suitable scan range to study the ORR on $La_{0.6}Sr_{0.4}MnO_3$. (a) CV of the $La_{0.6}Sr_{0.4}MnO_3$ disk during the 2nd cycle and (b) relative disk currents at 0.70 V vs. RHE during each of the scan ranges indicated by the lower voltage boundary. (c) The corresponding ring signal at 1.20 V vs. RHE during CV in the 2nd cycle and (d) relative smoothed ring currents at a disk voltage of 0.70 V vs. RHE during each of the scan ranges. (e) The peroxide yield during the 2nd cycle and (f) the smoothed peroxide yield at the disk voltage of 0.70 V vs. RHE during each of the scan ranges. The measurements were performed in O_2-saturated 0.1 M NaOH at 10 mV/s and 1600 rpm unless otherwise indicated. Thin lines in panels c and e indicate raw data and thick lines were smoothed by a 10 pt moving box average.

lower than 0.49 V vs. RHE. The measured current densities did not appear to be limited by mass transport in the investigated scan ranges at 1600 rpm (and higher rotation rates). These effects were also previously observed for the related (001)-oriented $La_{0.67}Sr_{0.33}MnO_3$ thin film[23] and polycrystalline $La_{0.8}Sr_{0.2}MnO_3$ film.[24]

The trends of the disk current on the number of cycles and overpotential was investigated during five cycles scanned in cathodic direction. We obtained the currents relative to those in the first cycle at reference voltages of 0.7 V vs. RHE (Figure 4b). At the lower voltage boundary of 0.69 V, there was no change discernable during five cycles. The next lower boundary voltage of 0.64 V vs. RHE showed a slight increase in the relative currents for three cycles, followed by a slight reduction back to the original value. At 0.59 V vs. RHE, the relative current did not change during the second cycle and then decreased. For all lower boundary voltages, the relative currents decreased by 6(1)% on average during each cycle (Table S2). Furthermore, a 50 mV decrease in the lower boundary resulted in a loss of 5% during the 5th cycle (Table S2). It should be noted that the absolute disk current densities also decreased for those lower boundary voltages (Figure 4a) so that the maximal current density was observed at 0.59 V vs. RHE. At a reference voltage of 0.8 V vs. RHE (Figure S5a), the activation above 0.69 V vs. RHE was more pronounced but we also found a loss of 6(1)% with cycling and 5% in current density for decrease of the lower boundary by 50 mV at the 5th cycle (Table S3). Therefore, the observed changes clearly depended on the voltage and manifested only below 0.7 V vs. RHE. We conclude that changes in the relative currents depended on both the number of cycles and the lower voltage boundary at any voltage below 0.7 V vs. RHE.

The observed changes at the disk correlated with the peroxide yield probed at the ring of the RRDE assembly (Figure 4c). The ring was set to 1.20 V vs. RHE to detect peroxide by oxidation.[51] While the disk was cycled five times, only four cycles could be analyzed at the ring due to a synchronization issue that we corrected during post-processing (Figure S4). The ring currents were congruent until a lower disk scan boundary of 0.69 V vs. RHE, after which they decreased. The relative (smoothed) ring currents suggest that the currents remained stable until 0.69 V vs. RHE (Figure 4d) akin to the relative disk currents. We note that the ring currents were noisier than the disk currents, which was also visible in the trends in Figure 4d and that the absolute ring currents also decreased below 0.69 V vs. RHE (Figure 4c). While the relative disk currents showed slight activation at 0.64 V vs. RHE, the relative ring currents at this boundary voltage and all lower voltages clearly decreased with 6% in current when the lower boundary was decreased by 50 mV, which is comparable to the disk (Table S4). However, the loss per cycle of 11(3)% was significantly higher as compared to the disk and the smallest relative ring current was 55% (Table S4), which is smaller than 71% at the disk (Table S2). The latter observation corroborated clearly and directly a voltage-dependent change in selectivity of the ORR on (001)-$La_{0.6}Sr_{0.4}MnO_3$ below 0.7 V vs. RHE.

The peroxide yield was consequently calculated using the method of Paulus et al.[51]: $X_{HO2} = \{2i_R/N\}/\{i_D + i_R/N\}$, where i_R is the ring current, i_D the disk current and N the collection efficiency. We determined an experimental collection efficiency of 41% (Figure S6), being within 1% of the expected 42%. The absence of currents due to manganese redox for an upper scan boundary of 1.0 V vs. RHE is supported by Figure 2, so that the disk currents correspond to the $4e^-$ reduction of O_2 to OH^- for vanishing ring currents. The calculated peroxide yields were between 75% and 55% above 0.7 V vs. RHE. Poux et al.[30] measured a maximum peroxide yield of about 50% near 0.7 V vs. RHE in 1 M NaOH at 900 rpm on $La_{0.8}Sr_{0.2}MnO_3$ powder. This deviation could be due to the presence of carbon in their study. A clear trend towards decreasing yield with lower voltage was found at lower potentials as also reported previously.[30] Yet, the minimum peroxide yield was about 40% for $La_{0.8}Sr_{0.2}MnO_3$ powder[30] at 0.4 V vs RHE, while it was as low as 10% on our $La_{0.6}Sr_{0.4}MnO_3$ thin films at this voltage (Figure 4e). Moreover, the yields at high voltages decreased for each of the shown curves, while all curves below 0.5 V vs. RHE fell onto each other,

suggesting that the material modification responsible for the change in selectivity had concluded below this voltage. The low peroxide yields at these high ORR overpotentials is attractive but we note that the disk currents (Figure 4a) unfortunately decreased much as compared to the pristine film.

The peroxide yields during each range varied less than the disk and ring currents individually. We studied the peroxide yield at two reference voltages, 0.7 and 0.8 V vs. RHE that were selected below and above of the threshold identified in Figure 3. At a disk voltage of 0.7 V vs. RHE (Figures 4f and S7a), the peroxide yield decreased during each cycle by an average of 2(1)% and 7% at the 5th cycle when the lower boundary was decreased by 50 mV (Table S5). At a disk voltage of 0.8 V (Figure S7b), the peroxide yield remained constant within the experimental spread (i.e. change by 1(3)%) during cycling and also decreased by 7% when the lower boundary was reduced by 50 mV (Table S6). Thus, the peroxide yield clearly depended on the overpotential at both reference voltages.

In summary, the peroxide yields were >50% up to a threshold disk voltage of 0.7 V vs. RHE when only the ORR was catalyzed, while the peroxide yields and total current decreased at lower voltages. The decreasing currents could be stopped or slowed by chemical modification as demonstrated by Risch et al.[25] Moreover, it is conceivable that the peroxide yields can be likewise controlled by chemical modifications as they depend on the manganese valence among other factors.[20,52,53] Whether structural or morphological changes occurred will be addressed below.

Bifunctional operation in devices such as metal-air or metal-O_2 batteries relies on catalysis of the OER in addition to the ORR. The OER on disks of $La_{0.6}Sr_{0.4}MnO_3$ thin films was previously studied by Scholz et al.[22,27] In their studies, both manganese rich and deficient films showed an increase in overpotential during the first ~20 cycles.[27] In contrast, Risch et al.[25] reported that the overpotential of the OER on unrotated $La_{0.8}Sr_{0.2}MnO_3$ thin films decreased during the first 20 cycles. After 100 cycles in an OER range (1.15 to 1.70 V vs. RHE), the films were cycled in an ORR range (1.00 to 0.65 V vs. RHE) where the ORR overpotential increased. Bifunctional cycling between ORR and OER (or *vice versa*) in a single cycle has not been systematically studied for thin films or composite electrodes in a wide voltage window.

We addressed this knowledge gap by repeating the systematic protocol on a pristine film (AFM in Figure S1b) where the lower voltage boundary was systematically decreased from 0.79 V to 0.39 V vs. RHE in 50 mV steps but with an upper voltage boundary of 1.74 V at which the OER was catalyzed (Figure 5a). In these experiments, the disk was first scanned in anodic direction from 0.99 V vs. RHE to 1.74 V vs. RHE and then in cathodic direction to varying lower voltage boundaries (Figure 5a). The onset of hysteresis occurred already at 0.59 V vs. RHE and was more pronounced as compared to the ORR-only investigations.

Several manganese redox peaks were detected in contrast to the investigation of the ORR only (Figure 4a). These peaks roughly correspond to those found for measurements in Ar-saturated NaOH (Figure 2 and S2a) and we thus assign peaks **i** to Mn^{2+} to Mn^{3+} oxidation, peak **ii** to Mn^{4+} to Mn^{3+} reduction and peaks **iii** to Mn^{3+} to Mn^{2+} reduction. In contrast to the measurements with fixed boundary voltages (Figure 2 and S2a), the position and width of peaks **i** and **iii** shifted when the lower voltage boundary was decreased, which we denote by one or more primes (i.e. **i'**, **iii'**, **iii''**) in Figure 5a. The appearance of peaks **i'** and **iii'** was clearly coupled as they occurred for voltage boundaries below 0.59 V vs. RHE. It has been discussed previously that the manganese valence strongly correlates with catalytic activity for both the ORR[20,32] and OER[1] where a valence between Mn^{3+} and Mn^{4+} is beneficial to both.[54]

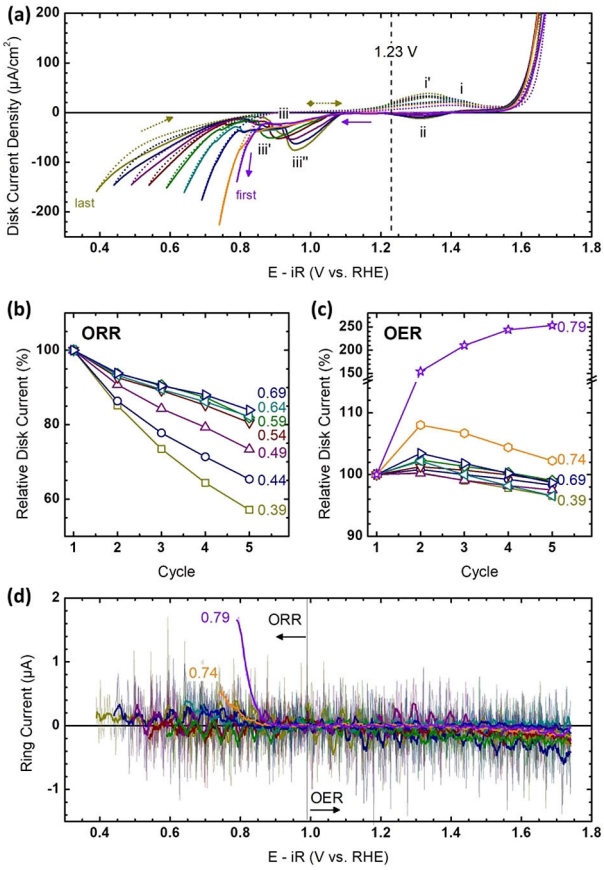

Figure 5. Identification of a suitable scan range for bifunctional cycling between OER and ORR on $La_{0.6}Sr_{0.4}MnO_3$. (a) CV of the $La_{0.6}Sr_{0.4}MnO_3$ disk during the 2nd cycle as well as relative disk currents at (b) 0.70 V vs. RHE and (c) 1.65 V vs. RHE during each of the scan ranges indicated by the lower voltage boundary. (d) The corresponding ring currents at 1.20 V vs. RHE. Thin lines indicate raw data and thick lines were smoothed by a 10 pt moving box average. The shown measurements were performed in O_2-saturated 0.1 M NaOH at 10 mV/s and 1600 rpm.

The activity of both the OER and ORR depended on whether the other reaction had also been performed and/or the intermediate redox peaks. The least changes were observed for the OER where the voltage at 100 $\mu A/cm^2_{ox}$ reduced from 1.65 to 1.63 V vs. RHE. The ORR currents decreased each time when the lower scan boundary was reduced. However, the minimal voltage of both films at 100 $\mu A/cm^2_{ox}$ did not initially depend on whether the OER had been performed (0.80 V vs. RHE; Figure 5a) or not (0.79 V vs. RHE; Figure 4a). There was a clear correlation with the height and position of peaks **iii** with

the reduction of the disk current density due to ORR such that greater peak height and higher voltage of the peak position both lead to lower ORR current density.

The trends of the disk current densities during ORR in OER-ORR cycling differ from those discussed above for ORR-only operation. In the former experiment, the relative ORR currents decayed with cycling at any lower voltage boundary (Figure 5b). Up to and including a lower boundary voltage of 0.54 V vs. RHE, the relative disk currents during ORR lost 4% during each cycle and there was no dependence on the lower boundary voltage (Table S7). Yet, the absolute current densities decreased. The loss during cycling increased at lower boundary voltages to up to 11% at 0.39 V vs. RHE (Table S7). In contrast, the relative OER currents increased with cycling (Figure 5c). At a lower boundary of 0.79 V vs. RHE, this enhancement is up to 253% at the 5th cycle (Table S8). All lower boundary voltages show the highest relative disk current during the 2nd cycle, after which the relative current loses 1% per cycle (Table S8). Overall, catalyzing the OER is less affected by the lower voltage boundary than the catalyzing the ORR.

The peroxide yield decreased during ORR-OER cycling as compared to ORR-only operation. Clear positive (smoothed) ring currents (i.e. peroxide) could only be resolved for lower boundaries of 0.79 and 0.74 V vs. RHE during ORR (Figure 5d). During OER, we could not detect any clear trends of positive currents assignable to peroxide or negative currents assignable to manganese dissolution. The apparent decrease of the dark blue trace was only detected during the 2nd cycle and could be a minor modification of the background currents (Figure S8), thus we focus on the evaluation of the peroxide yield during ORR for the above voltage boundaries (Figure S7c). At 0.79 V vs. RHE, the peroxide yield decreased from 52% by 11% per cycle to 19% after 4 cycles (Table S9). At 0.74 V vs. RHE, the yield decreased further to a steady level of 8(1)%. In contrast, the yields at 0.74 V were 65% during ORR-only operation (Figure S7b). This demonstrated clearly that including the OER range lowered the peroxide yield drastically.

There were only minor changes to morphology and roughness during either ORR-only or OER-ORR cycling, which we probed by *post mortem* AFM (Figure 6a,b) and *in situ* electrochemical cycling in a capacitive region (Figure 6c,d). The terrace structure and decorations were preserved after our experiments as shown by AFM (Figure 6a,b). The shown spots had RMS values of 0.4 nm for ORR-only and 0.2 nm for OER-ORR cycling, which corresponded to 342% and 164% relative to the 0.1 nm of the pristine films (Figure S1). The roughness factors were 1.00071 and 1.00020, which was again larger than the 1.00007 and 1.00009 of the pristine films. These changes were only qualitative because only a small fraction of the surface was probed. In a complementary experiment, we thus determined the relative changes of the entire electrode by cyclic voltammetry in a small voltage window, where ideally only the double layer capacitance was probed. We performed these measurements before the catalytic investigations and after each change of the voltage boundary. It is conceivable that the observed deviations from the expected box shape (such as the grey trace in Figure 6d) were caused by manganese redox. Yet, these

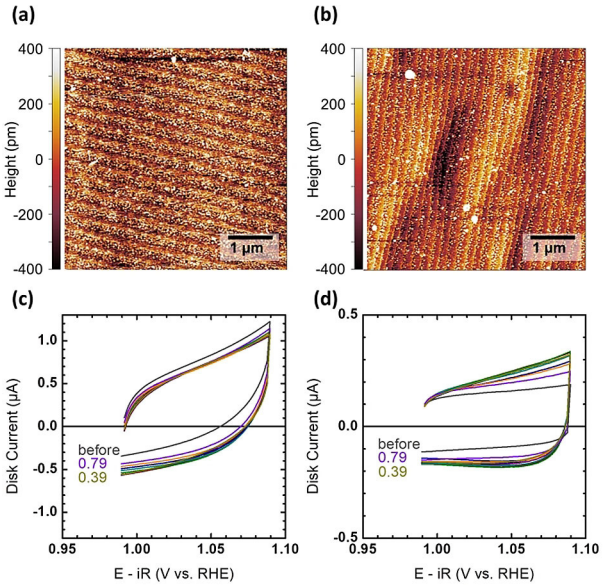

Figure 6. Surface morphology of (001)-$La_{0.6}Sr_{0.4}MnO_3$ (a) after cycling with the ORR-only protocol (data in Figure 4) and (b) after bifunctional OER-ORR cycling (data in Figure 5). CVs probing the initial double layer capacitance after each lowering of the voltage boundary during (c) the ORR-only protocol and (d) during OER-ORR cycling. The shown measurements were performed during the 2nd cycle in O_2-saturated 0.1 M NaOH at 10 mV/s and 1600 rpm.

changes were small and no new peaks arose. The measured currents should thus increase with growing surface area. We evaluated the average of the absolute anodic and cathodic currents in the middle of the voltage window at 1.03 V vs. RHE to be insensitive to vertical shifts of the curves. The relative currents before catalytic cycling to after the final step with a lower boundary of 0.39 V vs. RHE were 113% for ORR-only and 147% for OER-ORR cycling. This suggested that the latter experiment resulted in a rougher surface, in contrast to our AFM results. Alternatively, it may be due to changes in the manganese redox activity, e.g., due to chemical reactions involving defects, which were coupled to the Mn redox processes as discussed below.

In summary, epitaxial $La_{0.6}Sr_{0.4}MnO_3$ films were investigated during ORR and bifunctional OER-ORR cycling. These films did not require any additives, which could act as co-catalysts[9,18] and were previously investigated extensively for OER.[22,27] Herein, the scan range greatly impacted the observed redox peaks as well as the catalytic activity and selectivity of the ORR. When only the ORR was investigated, the CV curves did not depend on the lower voltage boundary of the scan range above 0.69 V vs. RHE and showed the expected current densities per oxide area. Continued reduction of the current density was found for lower boundary voltages during ORR-only and in any range during OER-ORR cycling. In the latter investigation, the OER currents more than doubled when the lower voltage boundary was 0.79 V vs. RHE and preserved this enhancement for any investigated scan range.

The general morphology was preserved throughout the experiments despite these clear changes in current density,

which cannot be explained by the observed minor roughening of the surface (OER trend) or contradict it (ORR trends). Therefore, we assign the observed changes in the CV curves to chemical modifications of $La_{0.6}Sr_{0.4}MnO_3$, i.e., changes in the manganese valence and compositional changes that need to be investigated further by additional methods.

No manganese redox was found when only the ORR was investigated or only the OER.[22,27] It is thus a reasonable assumption that manganese in $La_{0.6}Sr_{0.4}MnO_3$ had the expected valence of close to $Mn^{3.4+}$ when either reaction is studied separately. Thus, we propose that the observed decrease in current densities must have additional origins such as chemical manganese redox or compositional changes. La enrichment coupled to Mn depletion was found after the OER was catalyzed[22,27] and oxygen vacancies were proposed to be introduced by the ORR for related $La_{0.8}Sr_{0.2}MnO_3$ thin films,[23] which renders compositional changes the most likely cause of the decreasing current densities. It could be alleviated by stabilizing the elements that are lost as reported for $Ba_{0.5}Sr_{0.5}Co_{0.8}Fe_{0.2}O_{3-\delta}$ on $La_{0.8}Sr_{0.2}MnO_3$.[25]

For OER-ORR cycling, manganese redox peaks were clearly resolved. These redox peaks suggest that an unknown fraction of Mn^{3+} was oxidized to Mn^{4+} before the OER and Mn^{3+} was reduced to Mn^{2+} before the ORR. This is unexpected for conductive $La_{0.6}Sr_{0.4}MnO_3$[22] with delocalized electronic states and may indicate the presence of charge localization in the space charge layer of the oxide semiconductor or due to defects such as oxygen vacancies.[23] Scholz et al.[22] reported a change of surface stoichiometry after cycling in the OER region, where Mn and Sr leaching led to a surface enrichment with La. Since no change in oxygen stoichiometry was observed, it was interpreted as a $V_{Mn}''''/D_{La}^{\bullet\bullet\bullet}$ defect couple (in Kroger-Vink notation[55]). Such an irreversible process may influence the defect reactions under more reductive conditions during ORR, and turn them from a (quasi-)reversible $Mn^{3+/2+}$ redox reaction to the irreversible formation of the $Mn_{Mn}'/^1/_2\ V_O^{\bullet\bullet}$ defect couple under Mn deficient surface conditions, which is not expected and observed under oxidative conditions (such as the OER). Indeed, the strong shift of the peaks **iii** in Figure 5a to more negative potentials may indicate an oxygen depletion of the surface, in agreement with studies of oxygen intercalation in another perovskite.[56] Therefore, the manganese valence during OER-ORR cycling likely differed as compared to separate investigations of only the ORR or only the OER. The quantitative calculation of the exact valences requires operando spectroscopy, which is beyond the scope of this report.

Our RRDE setup allowed quantification of the peroxide yield, which was previously unknown for thin films of the $La_{1-x}Sr_xMnO_3$ perovskites. The peroxide yield was larger than 50% in the range 0.69 V to 0.99 V vs. RHE, where the ORR could be investigated without reduction of the current density. The desired lower peroxide yields were only observed at high overpotential for the ORR where they approached 10% below 0.50 V vs. RHE. Surprisingly, the peroxide yields were drastically reduced during bifunctional OER-ORR cycling where we found 8(1)% peroxide yield already at 0.8 V vs. RHE in the range 0.74 to 1.74 V vs. RHE. The observed redox peaks suggested that manganese was oxidized during OER-ORR cycling and we hypothesize that a higher valence as compared to the ORR-only protocol reduces the peroxide yield. This is supported by a previous study[53] of $La_{1-x}Sr_xMnO_3$ powders where intermediate $Mn^{3+/4+}$ mixtures resulted in the lowest peroxide yield. A recent review[20] concluded that Mn^{3+} is a requirement for low peroxide yield where some Mn^{4+}, but not Mn^{2+}, mixtures may reduce the peroxide yield, which also agrees with our data. As we argued above that the formation of Mn^{2+} is likely coupled to oxygen vacancies, it is conceivable that oxygen vacancies enhance the peroxide yield. Overall, we recommend the range of 0.74 V to 1.74 V vs. RHE for further, potentially long-term studies, of bifunctional OER-ORR operation of the (001)-$La_{0.6}Sr_{0.4}MnO_3$ surface because the OER activity was optimal, the ORR activity was second best and the peroxide yield was low.

3. Conclusions

We discussed the oxygen reduction reaction and bifunctional cycling between oxygen evolution and oxygen reduction on (001)-oriented $La_{0.6}Sr_{0.4}MnO_3$. The ideal scan ranges, in particular the lower voltage boundary, differed for ORR-only and OER-ORR cycling. Yet, no significant changes of the surface morphology were observed even for scan ranges that did not result in reproducible CV traces. Manganese redox peaks were only observed during OER-ORR cycling. Thus, we assigned the observed increase in OER activity and decrease in ORR activity to changes of the manganese valence probably coupled to defect chemical reactions. The valence changes also had drastic impact on the peroxide yield, which was well above 50% during the ORR only investigation and approached 8(1)% for OER-ORR cycling at 0.8 V vs. RHE. We assigned this desirable reduction to manganese oxidation. Overall, our study demonstrated the importance of the electrode history, e.g. due to valence changes, for bifunctional investigations. A new electrocatalyst for OER-ORR cycling can thus not be predicted by studies that considered each reaction separately. This insight is important to develop appropriate benchmarking protocols for bifunctional OER-ORR cycling and ultimately to predict better bifunctional catalysts.

Experimental Section

The $La_{0.6}Sr_{0.4}MnO_3$ (LSMO) films were prepared by ion-beam sputtering as reported previously, albeit with an optimized temperature.[22,27,35] The substrate was 0.5 wt% Nb-doped $SrTiO_3$, i.e., $SrNb_{0.003}Ti_{0.997}O_3$ (STNO) purchased from CrysTec GmbH and used as received. The films were deposited at 750 °C in an oxygen atmosphere of 1.7×10^{-4} mbar. The prepared films were kept under preparation conditions for 30 min, then slowly cooled down to room temperature, including a resting point of 30 min at 500 °C to reduce the number of defects. These parameters were selected to yield films of nominally 80 nm thickness as reported previously.[22]

The assembly of the RRDE electrodes is described in detail in ref. [22]. In short, carbon tape and InGa eutectic (Sigma-Aldrich, 99.99%) served as the flexible and adjustable conductive spacer. In the final assembly, only the thin film surface is exposed to the

electrolyte after fixation with chemically-stable, nonconductive epoxy (Omegabond 101).

XRD patterns were obtained using a Bruker D8 diffractometer with a monochromatized Cu–Kα source. The surface morphology was characterized by atomic force microscopy (AFM) using a MFP-3D Classic (Asylum Research) in tapping mode. The root mean squared roughness (RMS) was calculated using the Gwyddion software[57] to quantify surface morphology. Additionally, an effective roughness factor was determined by dividing the three-dimensional surface area by the projected area as described in ref. [25], where the former was obtained by a triangulation method in Gwyddion.

The electrochemical measurements were carried out with two Interface 1000E (Gamry Instruments Inc.) in a bipotentiostat setup and an RRDE-3 A rotator (ALS Co. Ltd.). The rotating ring electrode consists of a disk electrode of the assembled $La_{0.6}Sr_{0.4}MnO_3$ electrode with a diameter of 4 mm and a Pt ring electrode with an inner diameter of 5 mm and an outer diameter of 7 mm. We found an experimental collection efficiency of 41% for this assembly using the ferri-/ferrocyanide redox couple (Figure S6). If not otherwise noted, the electrochemical measurements were performed in 0.1 M NaOH electrolyte prepared by diluting NaOH stock solution (Sigma Aldrich) with deionized water (MilliQ, >18.2 MΩ). The electrolyte was saturated with O_2 or Ar gas at least 30 min before measurements and continuously purged with these gases throughout the measurement. CVs of the Pt ring were recorded in the hydrogen underdeposition region using first a commercial reversible hydrogen electrode (RHE; Gaskatel GmbH) and then immediately afterwards using a commercial Hg/HgO reference electrode (ALS Co. Ltd.) filled with 1 M NaOH (Figure S9). The offset between these two measurements was used to convert the disk voltages measured with the Hg/HgO electrode to the RHE scale.

The measurement protocol consisted of two main parts. First, an initial AC impedance spectroscopy measurement, then the electrochemical characterization, which includes CVs in a 0.1 V range (Figure 6c,d) with different scan rates (250, 200, 150, 100, 50, 40, 30, 20, 10 mV/s) to probe the double layer capacitance. The characterization protocol was performed before and after the second part, namely the catalytic investigation. The disk and ring were first held at their starting potentials for 120 s, then the disk was swept in a certain voltage range, while the ring was held at 1.20 V vs. RHE. If not otherwise noted, the RRDE was rotated at 1600 rpm. Pristine electrodes were measured without prior activation. The ORR-only measurements were repeated once with identical trends on a rougher film.[58] The OER-ORR cycling protocol was not exactly reproduced but the final range was studied for multiple cycles (Figure S2) and yielded comparable results. Charges were obtained by integration of the currents in CV on a voltage axis, which was then converted to charge by division of the sweep speed (10 mV/s). The value of the obtained charges depended slightly on the choice of the baseline. Finally, the peroxide yield was calculated using the method of Paulus et al.[51]

Acknowledgements

Financial support by the Deutsche Forschungsgemeinschaft (DFG Sachbeihilfe RI 2777/3 and SFB 1073, project C02) is gratefully acknowledged.

Conflict of Interest

The authors declare no conflict of interest.

Keywords: bifunctional catalysts · model electrode · oxygen reduction · peroxide · RRDE

[1] W. T. Hong, M. Risch, K. A. Stoerzinger, A. J. L. Grimaud, J. Suntivich, Y. Shao-Horn, *Energy Environ. Sci.* **2015**, *8*, 1404–1427.
[2] I. Katsounaros, S. Cherevko, A. R. Zeradjanin, K. J. J. Mayrhofer, *Angew. Chem. Int. Ed. Engl.* **2014**, *53*, 102–21.
[3] Y.-J. Wang, B. Fang, D. Zhang, A. Li, D. P. Wilkinson, A. Ignaszak, L. Zhang, J. Zhang, *Electrochem. Energy Rev.* **2018**, *1*, 1–34.
[4] Z.-F. Huang, J. Wang, Y. Peng, C.-Y. Jung, A. Fisher, X. Wang, *Adv. Energy Mater.* **2017**, *7*, 1700544.
[5] R. Cao, J.-S. Lee, M. Liu, J. Cho, *Adv. Energy Mater.* **2012**, *2*, 816–829.
[6] S. Gupta, W. Kellogg, H. Xu, X. Liu, J. Cho, G. Wu, *Chem. – An Asian J.* **2016**, *11*, 10–21.
[7] D. Chen, C. Chen, Z. M. Baiyee, Z. Shao, F. Ciucci, *Chem. Rev.* **2015**, *115*, 9869–9921.
[8] L. Jörissen, *J. Power Sources* **2006**, *155*, 23–32.
[9] Y. Zhu, W. Zhou, Z. Shao, *Small* **2017**, *13*, 1603793.
[10] J. Pan, X. L. Tian, S. Zaman, Z. Dong, H. Liu, H. S. Park, B. Y. Xia, *Batter. Supercaps* **2018**, DOI 10.1002/batt.201800082.
[11] D. U. Lee, P. Xu, Z. P. Cano, A. G. Kashkooli, M. G. Park, Z. Chen, *J. Mater. Chem. A* **2016**, *4*, 7107–7134.
[12] S. R. Narayan, A. Manohar, S. Mukerjee, *Interface Mag.* **2015**, *24*, 65–69.
[13] J.-I. Jung, M. Risch, S. Park, M. G. Kim, G. Nam, H.-Y. Jeong, Y. Shao-Horn, J. Cho, *Energy Environ. Sci.* **2016**, *9*, 176–183.
[14] E. Davari, D. G. Ivey, *Sustain. Energy Fuels* **2018**, *2*, 39–67.
[15] Y. Li, M. Gong, Y. Liang, J. Feng, J.-E. Kim, H. Wang, G. Hong, B. Zhang, H. Dai, *Nat. Commun.* **2013**, *4*, 1805.
[16] J. Suntivich, K. J. May, H. A. Gasteiger, J. B. Goodenough, Y. Shao-Horn, *Science* **2011**, *334*, 1383–1385.
[17] J. Suntivich, H. A. Gasteiger, N. Yabuuchi, H. Nakanishi, J. B. Goodenough, Y. Shao-Horn, *Nat. Chem.* **2011**, *3*, 546–50.
[18] M. Risch, *Catalysts* **2017**, *7*, 154.
[19] D. Mierwaldt, S. Mildner, R. Arrigo, A. Knop-Gericke, E. Franke, A. Blumenstein, J. Hoffmann, C. Jooss, *Catalysts* **2014**, *4*, 129–145.
[20] K. A. Stoerzinger, M. Risch, B. Han, Y. Shao-Horn, *ACS Catal.* **2015**, *5*, 6021–6031.
[21] K. A. Stoerzinger, W. Lü, C. Li, Ariando, T. Venkatesan, Y. Shao-Horn, *J. Phys. Chem. Lett.* **2015**, *6*, 1435–1440.
[22] J. Scholz, M. Risch, K. A. Stoerzinger, G. Wartner, Y. Shao-Horn, C. Jooss, *J. Phys. Chem. C* **2016**, *120*, 27746–27756.
[23] D. Kan, Y. Orikasa, K. Nitta, H. Tanida, R. Kurosaki, T. Nishimura, T. Sasaki, H. Guo, Y. Ozaki, Y. Uchimoto, *J. Phys. Chem. C* **2016**, *120*, 6006–6010.
[24] Y. Miyahara, K. Miyazaki, T. Fukutsuka, T. Abe, *J. Electrochem. Soc.* **2014**, *161*, F694–F697.
[25] M. Risch, K. A. Stoerzinger, S. Maruyama, W. T. Hong, I. Takeuchi, Y. Shao-Horn, *J. Am. Chem. Soc.* **2014**, *136*, 5229–5232.
[26] K. A. Stoerzinger, M. Risch, J. Suntivich, W. M. Lü, J. Zhou, M. D. Biegalski, H. M. Christen, Ariando, T. Venkatesan, S.-H. Yang, *Energy Environ. Sci.* **2013**, *6*, 1582–1588.
[27] J. Scholz, M. Risch, G. Wartner, C. Luderer, V. Roddatis, C. Jooss, *Catalysts* **2017**, *7*, 139.
[28] X. Shi, S. Siahrostami, G.-L. Li, Y. Zhang, P. Chakthranont, F. Studt, T. F. Jaramillo, X. Zheng, J. K. Nørskov, *Nat. Commun.* **2017**, *8*, 701.
[29] M. Risch, K. A. Stoerzinger, B. Han, T. Z. Regier, D. Peak, S. Y. Sayed, C. Wei, Z. J. Xu, Y. Shao-Horn, *J. Phys. Chem. C* **2017**, *121*, 17682–17692.
[30] T. Poux, A. Bonnefont, G. Kéranguéven, G. A. Tsirlina, E. R. Savinova, *ChemPhysChem* **2014**, *15*, 2108–20.
[31] S. Malkhandi, P. Trinh, A. K. Manohar, K. C. Jayachandrababu, A. Kindler, G. K. Surya Prakash, S. R. Narayanan, *J. Electrochem. Soc.* **2013**, *160*, F943–F952.
[32] T. Poux, F. S. Napolskiy, T. Dintzer, G. Kéranguéven, S. Y. Istomin, G. A. Tsirlina, E. V. Antipov, E. R. Savinova, *Catal. Today* **2012**, *189*, 83–92.
[33] T. Li, J. Liu, X. Jin, F. Wang, Y. Song, *Electrochim. Acta* **2016**, *198*, 115–126.
[34] R. H. Mitchell, A. R. Chakhmouradian, P. M. Woodward, *Phys. Chem. Miner.* **2000**, *27*, 583–589.
[35] J. Odrobina, J. Scholz, M. Risch, S. Dechert, C. Jooss, F. Meyer, *ACS Catal.* **2017**, *7*, 6235–6244.
[36] K. Zhang, X. Han, Z. Hu, X. Zhang, Z. Tao, J. Chen, *Chem. Soc. Rev.* **2015**, *44*, 699–728.
[37] A. M. Gómez-Marín, R. Rizo, J. M. Feliu, *Catal. Sci. Technol.* **2014**, *4*, 1685.
[38] Y.-F. Huang, M. T. M. Koper, *J. Phys. Chem. Lett.* **2017**, *8*, 1152–1156.
[39] V. Climent, J. M. Feliu, Wiley-Blackwell, **2017**, pp. 1–57.

[40] Y. Gorlin, B. Lassalle-Kaiser, J. D. Benck, S. Gul, S. M. Webb, V. K. Yachandra, J. Yano, T. F. Jaramillo, *J. Am. Chem. Soc.* **2013**, *135*, 8525–34.
[41] F. H. B. Lima, M. L. Calegaro, E. A. Ticianelli, *Electrochim. Acta* **2007**, *52*, 3732–3738.
[42] A. J. Grutter, D. A. Gilbert, U. S. Alaan, E. Arenholz, B. B. Maranville, J. A. Borchers, Y. Suzuki, K. Liu, B. J. Kirby, *Appl. Phys. Lett.* **2016**, *108*, 082405.
[43] M. P. de Jong, I. Bergenti, W. Osikowicz, R. Friedlein, V. A. Dediu, C. Taliani, W. R. Salaneck, *Phys. Rev. B* **2006**, *73*, 052403.
[44] R. Zhao, K. Jin, Z. Xu, H. Guo, L. Wang, C. Ge, H. Lu, G. Yang, *Appl. Phys. Lett.* **2013**, *102*, 122402.
[45] C. Yang, A. Grimaud, *Catalysts* **2017**, *7*, 149.
[46] J. Norpoth, S. Mildner, M. Scherff, J. Hoffmann, C. Jooss, *Nanoscale* **2014**, *6*, 9852–9862.
[47] S. Raabe, D. Mierwaldt, J. Ciston, M. Uijttewaal, H. Stein, J. Hoffmann, Y. Zhu, P. Blöchl, C. Jooss, *Adv. Funct. Mater.* **2012**, *22*, 3378–3388.
[48] V. Celorrio, L. Calvillo, G. Granozzi, A. E. Russell, D. J. Fermin, *Top. Catal.* **2018**, 1–8.
[49] V. Celorrio, L. Calvillo, E. Dann, G. Granozzi, A. Aguadero, D. Kramer, A. E. Russell, D. J. Fermín, *Catal. Sci. Technol.* **2016**, *6*, 7231–7238.
[50] V. Celorrio, E. Dann, L. Calvillo, D. J. Morgan, S. R. Hall, D. J. Fermin, *ChemElectroChem* **2016**, *3*, 283–291.
[51] U. A. Paulus, T. J. Schmidt, H. A. Gasteiger, R. J. Behm, *J. Electroanal. Chem.* **2001**, *495*, 134–145.
[52] I. Roche, E. Chaînet, M. Chatenet, J. Vondrák, *J. Phys. Chem. C* **2007**, *111*, 1434–1443.
[53] J. Tulloch, S. W. Donne, *J. Power Sources* **2009**, *188*, 359–366.
[54] A. S. Ryabova, F. S. Napolskiy, T. Poux, S. Y. Istomin, A. Bonnefont, D. M. Antipin, A. Y. Baranchikov, E. E. Levin, A. M. Abakumov, G. Kéranguéven, et al., *Electrochim. Acta* **2016**, *187*, 161–172.
[55] F. A. Kröger, H. J. Vink, *J. Phys. Chem. Solids* **1958**, *5*, 208–223.
[56] A. Nemudry, P. Rudolf, R. Schöllhorn, *Chem. Mater.* **1996**, *8*, 2232–2238.
[57] D. Nečas, P. Klapetek, *Open Phys.* **2012**, *10*, 181–188.
[58] L. Köhler, Untersuchungen Der Sauerstoffelektrokatalyse an Epitaktischen La0.6Sr0.4MnO3 Dünnfilmen, Georg-August Universität Göttingen, **2018**.

Manuscript received: November 2, 2018
Revised manuscript received: December 3, 2018
Accepted manuscript online: December 4, 2018
Version of record online: January 29, 2019